Physics prospects with the ATLAS detector at the LHC

Saúl González
University of Wisconsin
Madison, WI 53706 USA

Abstract

The LHC will be the next premier discovery facility for High Energy Physics with a center-of-mass energy of 14 TeV and very high luminosity. The ATLAS detector, one of two general purpose detectors proposed for the LHC, will exploit this new potential with a design optimized to answer the most pressing questions in High Energy Physics today. In this talk, an overview of the issues and prospects with ATLAS for discovery of the Standard Model or MSSM Higgs bosons and discovery and measurement of SUSY particles will be given, as well as the expectations for B-physics measurements.

1 Introduction

Much progress has been made in Particle Physics in the last 30 years, and yet, one of the most fundamental question in the context of Electroweak theory remains to be answered. The "origin of mass" problem is the main motivation for constructing the Large Hadron Collider (LHC) and its associated detectors. While there is no assurance that the Electroweak symmetry breaking mechanism will be experimentally confirmed at the LHC, the new energy and luminosity frontiers reached by this machine guarantee that definitive statements can be made about the existence of the minimal Standard Model Higgs.

This new frontier will also allow decisive tests of extensions to the Standard Model. In addition to the Higgs sector, supersymmetric particle partners may provide immediate and striking evidence for one of the SUSY-inspired models. In particular, detailed measurements can be made of cross sections, branching fractions, and particle masses in the context of the minimal supersymmetric extension of the Standard Model (MSSM). These precision measurements can in turn be used to discriminate among competing models.

By virtue of its high luminosity, the LHC will also be a B factory. Various topics in B physics will be studied in detail by using fully reconstructed B decay modes. These studies complement the search and discovery program by further probing of the Standard Model parameters. A dedicated vertex detector will allow ATLAS to perform precision measurements, including CP violation, rare decays, and B_s mixing.

Many other topics will be studied at the LHC. The common signatures for which the ATLAS detector has been optimized (*eg,* $\not\!\!E_T$, leptons, jets) will be used to search for other new phenomena. Among these are resonances arising from technicolor models, strongly interacting Higgs, heavy gauge bosons, leptoquarks, compositeness, and new heavy quarks or leptons. There will also be detailed studies of top production and Standard Model measurements.

The aim of this talk is to give an overview of the physics prospects with the ATLAS detector at the LHC. Due to the time limitations, and the breadth of this subject, this presentation only covers search for Standard Model and MSSM Higgs, SUSY searches and measurements, and B physics.

2 Evaluating Physics reach

The ATLAS physics prospects presented here have generally been obtained with a full detector simulation or by using the performance parameters derived from a full simulation. In some cases, a fast but accurate simulation of the ATLAS detector has been used. Most signal and background physics processes, unless otherwise noted, have been simulated with PYTHIA 5.7 [1] at a center-of-mass energy of 14 TeV. Initial- and final-state radiation, hadronization, and particle decays were also simulated with PYTHIA. Much advance has been made recently in the calculation of higher-order QCD corrections ("K-factors") to signal processes at LHC energies. However, at the time of these studies, the corrections for all background processes had not been completed. Thus, for the sake of consistency, all the following results do not include K-factor corrections unless otherwise noted. It is important to note that some of these corrections can amount to 50–100% [2] of the total cross section values. When talking about "reach" for a particular physics channel, the significance $S/\sqrt{B}$, where S is the number of "signal" events and B is the number of background events, will be used to quantify its potential. The arbitrary criteron for discovery used here is $S/\sqrt{B} \geq 5$.

3 ATLAS at the LHC

3.1 The machine and the detector

The LHC [3], a proton on proton collider designed to sit in CERN's LEP tunnel, is scheduled to start operating in the year 2005. The scheduled center-of-mass energy at turn-on is 14 TeV with a bunch crossing rate of 40 MHz and an initial ("low") luminosity of $\mathcal{L} \approx 10^{33}\mathrm{cm}^{-2}\mathrm{s}^{-1}$. After some years of low luminosity running, the collider luminosity will be upgraded to $\mathcal{L} \approx 10^{34}\mathrm{cm}^{-2}\mathrm{s}^{-1}$. The low rate of simultaneous interactions ("pilepup") during the low lumonosity period will provide the right conditions for B physics studies.

In order to obtain a realistic evaluation of the ATLAS physics potential, in this talk we assume a "conservative" luminosity profile consisting of three years at low luminosity and all running beyond this initial period at peak luminosity. We will refer to these periods as the low integrated luminosity ($3{\times}10^4\mathrm{pb}^{-1}$, first three years) and the peak integrated luminosity scenarios ($3{\times}10^5\mathrm{pb}^{-1}$, first four years), respectively.

The ATLAS detector is in its final design stage. Many of the subdetector designs have been finalized and their Technical Design Reports (TDR) recently completed [4]. A detailed description of the ATLAS detector can be found in these documents and in the original Technical Proposal [5]. In addition, recent information on the status of the ATLAS detector can be found elsewhere in this Workshop [6]. Here, only a brief description of the more relevant elements of the ATLAS detector will be given.

ATLAS has been designed as a general purpose detector optimized for both discovery and precision measurement physics. The tracking system consists of an Inner Detector (ID) in a 2 Tesla solenoidal magnetic field and a muon spectrometer in a large toroidal magnet system. The muon spectrometer occupies the bulk of the ATLAS volume.

The Inner Detector consists of a Semiconductor Tracker (SCT) and a Transition Radiation Tracker (TRT). The SCT has two pixel detector layers and four silicon strip detector layers with pseudorapidity coverage of $|\eta| < 2.5$. An extra pixel layer (the "B layer"), close to the beam-pipe, will provide an additional precision point during the initial low luminosity run. The TRT consists of straw tubes providing 35 $r - \phi$ hits and electron identification.

The ATLAS calorimeter has been designed to be hermetic to $|\eta| < 5$. A liquid argon calorimeter in a barrel-endcap geometry provides good electromagnetic (EM) energy resolution and good radiation hardness. Fine-segmented presamplers help in π^0 rejection. Hadronic calorimetry is provided by a barrel scintillator-tile calorimeter and an endcap LAr calorimeter.

A flexible three level trigger system ensures that the data rates will be manageable for both the low and high luminosity running periods.

3.2 Pileup Issues at the LHC

At the center-of-mass energy of 14 TeV, the total inelastic and non-diffractive cross section is about 70 mb. With a bunch rate of 40 MHz and at peak luminosity, this translates into approximately 18 interactions per bunch crossing or more, depending on the subdetector timing. These pileup events in turn degrade analysis quantities like $\not{E}_{\mathrm{T}}$, lepton isolation, jet reconstruction, and others. It is thus important to evaluate the reach of a particular analysis at the different instantaneous luminosity scenarios. In addition, one has to consider that detector components will physically deteriorate as the radiation fluence increases. In particular, the B layer will be removed at the end of the low luminosity run, diminishing the B-tagging capabilities of the detector.

4 Standard Model Higgs

4.1 Introduction

If the Standard Model fundamental particles are to remain weakly-interacting at high energies, then the broken electroweak sector must contain at least one scalar Higgs boson. It is the discovery potential for Higgs which provides the main motivation for building the LHC. Higgs studies also provide a well-known benchmark to assess the physics reach in the LHC environment in terms of detector performance. Thus, many of the Higgs channels have been used in the optimization of the ATLAS detector design.

At present, the best limits on the SM Higgs mass come from the LEP1 and LEP2 direct searches [7] ($m_{\rm H}$ $>$ 77.5 GeV/c^2). Fits to Electroweak parameters [8] also favor a low mass Higgs ($m_{\rm H} <$ 430 GeV/c^2 at 95% confidence level). At the time of LHC turn-on TeV33 [9] will have the best reach with a Higgs discovery potential of $m_{\rm H}$ $<$ 120 GeV/c^2 .

4.2 SM Higgs production and decay

Higgs production at the LHC happens mainly via the Higgs preference to couple to heavy particles (W, Z, and top). Figure 1 shows the Higgs cross section [10] as a function of mass for the main production modes at $\sqrt{s} = 14$ TeV. Gluon-gluon fusion, through heavy quark loops, is by far the dominant production mechanism. The second highest production mode is via WW and ZZ fusion. In this case, the Higgs is accompanied by at least two jets which can be used as a tag in reducing the QCD backgrounds. The third mode is associated W or Z production. This mode can provide one of the cleanest experimental tags for Higgs production with the use of the leptonic decay of the W.

Like the production cross section, the Higgs decay branching ratios depend on the Higgs mass $m_{\rm H}$. For $m_{\rm H}$ <130 GeV/c^2 , the dominant decay mode is $\rm H \rightarrow b\bar{b}$. Above $2m_{\rm W}$, the decays are dominated by WW and ZZ final states with a $\rm t\bar{t}$ contribution for $m_{\rm H} > 2m_{\rm top}$. In the region $m_{\rm W} < m_{\rm H} < 2m_{\rm W}$ there is an order 10^{-3} contribution from $\rm H \rightarrow \gamma\gamma$. Although small, this final state has the very distinctive experimental signature of two high-$p_{\rm T}$ photons, making it well suited for the high luminosity environment at the LHC.

In the following, the ATLAS discovery reach for some of the different Higgs channels is discussed. Since the experimental signatures depend on $m_{\rm H}$, it is natural to identify two distinct regions of $m_{\rm H}$ in the discussion of reach: intermediate mass Higgs ($m_{\rm H} < 2m_{\rm W}$) and high mass Higgs ($m_{\rm H} > 2m_{\rm W}$). The summary of the reach for the SM Higgs is presented in Figure 3 for an integrated luminosity of 10^5pb^{-1}.

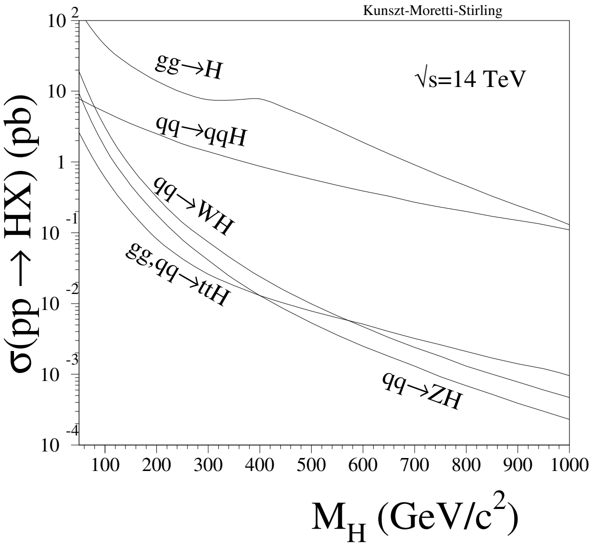

Figure 1: Cross section for Higgs production at 14 TeV.

4.3 The $\mathrm{H}\rightarrow\gamma\gamma$ channel

One of the most striking signatures for Higgs decay in the intermediate mass range comes from the channel $\mathrm{H}\rightarrow\gamma\gamma$. For a high Higgs mass, the $\mathrm{H}\rightarrow\gamma\gamma$ branching ratio is negligible. Although it has a small branching fraction, one can take advantage of the good electromagnetic calorimeter resolution to reject backgrounds. For a Higgs mass of 120 GeV/c^2, one expects about 5000 events produced in one year of running at peak luminosity [11]. The backgrounds to $\mathrm{H}\rightarrow\gamma\gamma$ have an irreducible component from continuum $\gamma\gamma$ production and reducible components from jet-jet, γ-jet, $\mathrm{Z}\rightarrow e^+e^-$, and Bremsstrahlung production.

The $\mathrm{H}\rightarrow\gamma\gamma$ reconstruction is basically a calorimeter measurement. Photons are identified in ATLAS by requiring an isolated cluster in the EM calorimeter with lateral and longitudinal shower shapes consistent with an electromagnetic energy deposition and by requiring no leakage into the hadronic calorimeter. By using the tracker, photon conversions can be identified and single electrons rejected. "Photon fakes", caused mainly by jets with energetic π^0s, are rejected by using the ATLAS presampler to reject "wide photons". A jet rejection of $R_{\mathrm{jet}} \approx 5000$ can be achieved with a total photon reconstruction efficiency of $\epsilon_\gamma \approx 80\%$. After these cuts, $\mathrm{H}\rightarrow\gamma\gamma$ events can be selected by requiring two high p_{T} photons (one with $p_{\mathrm{T}} > 40$ GeV/c and one with at least $p_{\mathrm{T}} > 25$ GeV/c) within the presampler region. After using the fine ATLAS calorimeter segentation to determine the photon direction, reconstruction efficiencies of 40–50% are obtained. Figure 2 shows the reconstructed di-photon mass for a 100 GeV/c^2 Higgs at high luminosity. The mass resolution at low luminosity, owing to the lower pileup contamination, is 30% better.

Three years at low luminosity are not enough to discover Higgs in this channel. At high luminosity, the reach for one year of running is $S/\sqrt{B} \approx 5$.

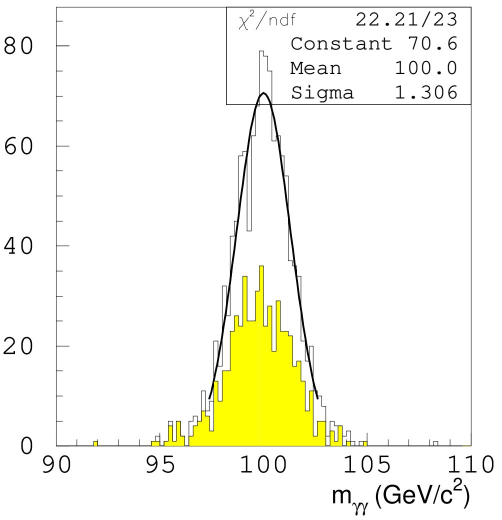

Figure 2: Reconstructed di-photon mass for $\mathrm{H}\rightarrow\gamma\gamma$ with $m_{\mathrm{H}} = 100$ GeV/c^2 (peak luminosity). The shaded region corresponds to events with at least one reconstructed photon conversion.

4.4 $\mathrm{H}\rightarrow\mathrm{b}\bar{\mathrm{b}}$

Although $\mathrm{H}\rightarrow\mathrm{b}\bar{\mathrm{b}}$ is the dominant Higgs decay mode for $m_{\mathrm{H}} < 130$ GeV/c^2, the high QCD backrounds makes it extremely difficult to extract a signal in this channel. And yet, this is an important mode since it has a significant overlap in mass reach with LEP2. The key in this case, as in LEP2, is in the use of b-tagging. In addition, since there is a significant cross section for Higgs production in association with a W, backgrounds are further reduced by tagging events with two b jets and a high p_{T} lepton from the W.

Events containing B mesons can be tagged in ATLAS by the use of an impact parameter tag [4]. The TRT and the SCT tracking information is used to form a signed impact parameter to identify jets with lifetime. The jet rejection of this tag as a function of efficiency has been determined from a full simulation of the ATLAS detector. For a tagging efficiency of ϵ_b =50%, the u-jet rejection us $R_u \approx$ 50–70 and the gluon jet rejection is $R_g \approx 30$. This tagging performance can still be improved by using the vertex z information and by rejecting secondaries. An additional b tagging technique is by the use of a soft lepton tag (SLT). The b quark decay $b \to e$ can be tagged by using the TRT's electron identification capabilities at low p_T ($p_T > 1$ GeV/c) and the EM calorimeter. The decay $b \to \mu$ for $p_T > 2$ GeV/c can be identified using the muon system and the hadron calorimeter. The SLT method gives an efficiency $\epsilon_b \approx$20% for a jet rejection of $R_{jet} \approx$100%. When combined with the impact parameter tag, a total b tagging efficiency of $\epsilon_b \approx$ 60% can thus be achieved.

The $H \to b\bar{b}$ events can then be selected by requiring one high p_T lepton and two b-tagged jets. The main backgrounds are from WZ, Wbb production (irreducible) and from Wjet-jet production (reducible). With an efficiency of $\epsilon_b \approx$ 60% and a jet rejection of $R_{jet} \approx$ 100% (achievable in ATLAS), the reach is $S/\sqrt{B} \approx 4.1$ for a m_H =100 GeV/c^2 Higgs at 3×10^4pb^{-1} . This is not enough, as in the case of $H \to \gamma\gamma$, to discover Higgs in the $H \to b\bar{b}$ channel alone.

4.5 $H \to 4\ell$

In the mass range 130 GeV/c^2 $< m_H <$ 180 GeV/c^2 , the most important Higgs decay mode is $H \to ZZ^* \to 4\ell$ [12]. The good mass resolution of ATLAS in the four lepton final state and good muon and electron identification capabilities are essential in rejecting background. The background consists mostly of $ZZ^* \to 4\ell$ (irreducible) and $t\bar{t}$, $Zb\bar{b}$ (reducible).

The $H \to 4\ell$ events are selected by requiring two high p_T leptons ($p_T >$20GeV/c) within $|\eta| < 2.5$ and two lower p_T leptons ($p_T >$7GeV/c). After rejecting leptons with lifetime and requiring that they be isolated, only events with a lepton pair consistent with a Z decay are kept. This selection yields large rejections: $R_{t\bar{t}} \approx 1000$ and $R_{Zb\bar{b}} \approx 100$. This translates to a reach of $S/\sqrt{B} \approx$ 5–20 for 3×10^4pb^{-1} .

In the high Higgs mass case, the four lepton channel is also very important. In this case, the four leptons are produced by two real Z's. The analysis is very similar as for the intermadiate mass case but the mass bins are adjusted to account for the larger Higgs width. Since the QCD backgrounds are greatly reduced at high mass, this is a very good channel for discovery of a massive Higgs at low luminosity. The reach is $S/\sqrt{B} \approx 5$ for 2×10^3pb^{-1} for a $m_H <$500 GeV/c^2 Higgs.

4.6 Other channels

In the high mass range, the Higgs decays predominantly to WW, ZZ, and $t\bar{t}$. The $t\bar{t}$ mode is very difficult to disentangle from the QCD background. However, the WW and ZZ mode can be identified by final states with electrons, muons, and neutrinos. In addition, the two accompanying jets in the $pp \to q\bar{q}H$ mode are used to further tag the event. The presence of neutrinos and very forward jets in the final state imposes the requirement of very good calorimeter coverage down to $|\eta| \approx 5$. Apart form the four lepton channel mentioned above, the final states considered are $ZZ \to \ell^+\ell^-\nu\bar{\nu}, \ell^+\ell^-$jet-jet and $WW \to \ell\nu$jet-jet. In the case of a final state with two neutrinos, the Higgs would be observed as an excess in the $\not{E}_T$ distribution. For example, for m_H = 700 GeV/c^2 , there would be an excess of events at $\not{E}_T \approx$300 GeV. The ATLAS detector coverage must then be large enough such that the pileup contribution is negligible at large $\not{E}_T$.

Figure 3 shows that the contributions from these channels is very significant at high m_H , and in fact dominate the reach for $m_H >$600 GeV/c^2 .

One can also see from Figure 3 that the Higgs mass range $m_H <1$ TeV/c^2 will be fully covered for an integrated luminosity of 10^5pb^{-1}, roughly corresponding to the first four years of LHC operation.

5 MSSM Higgs

5.1 Introduction

Supersymmetry provides a natural solution to the hierarchy problem in the Standard Model. In the Minimal Supersymmetric extension to the Standard Model, two Higgs doublets yield five scalar Higgs physical states: two neutral scalar CP-even h and H, a neutral CP-odd pseudoscalar A, and two charged

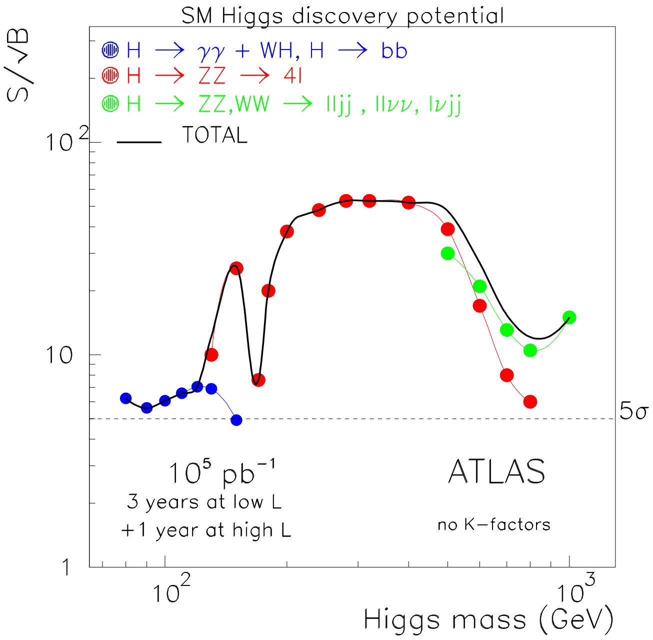

Figure 3: Summary of SM Higgs discovery potential during the first four years of operation at $\sqrt{s}$ = 14 TeV.

scalars $H^{\pm}$. At tree-level, the MSSM Higgs sector can be specified by two parameters, here taken as the ratio of the Higgs doublets VEV's $\tan\beta$ and the mass of the CP-odd Higgs m_A .

Many of MSSM neutral Higgs final states are very similar to those of the Standard Model Higgs except for the couplings, and thus production rates, which are modified by supersymmetric terms. Table 1 summarizes some of the MSSM channels which have been considered in ATLAS, along with their production mode and the main experimental tagging method. Those channels with complete overlap with the Stadard Model have been labled as "SM" in the table.

In calculating the MSSM Higgs reach of the ATLAS detector [13], the following working assumptions have been used: the SUSY scale $M_{SUSY} \approx 1$ TeV/c^2 so that no SUSY particles appear in the final state, there is negligible stop-sbottom mixing, and the higgsino mass parameter $|\mu| \approx 0$.

At tree-level, the MSSM mass relations imply that $m_h < m_Z$. After applying higher order corrections [14], the mass of the lightest MSSM Higgs is bound by $m_h < 112$ GeV/c^2 (for the above assumptions and for m_{top} =175 GeV/c^2). This upper bound is outside the discovery reach of LEP2 [15] of $m_h \approx 90$ GeV/c^2 . It is thus important, in searching for the lightest MSSM Higgs, to study the dominant decay modes for this mass range: $h \to \gamma\gamma$, $h \to b\bar{b}$, and $h \to 4\ell$.

In the following, the salient points for some of the studies of MSSM reach with the ATLAS detector will be shown for a few of the Higgs decay modes. Figures 4 and 5 summarize the ATLAS MSSM prospects for two luminosity scenarios and for m_{top} =175 GeV/c^2 . The figures also include the LEP2 MSSM reach for 150pb^{-1} at $\sqrt{s}$=192 GeV.

5.2 Standard Model-like channels

The issues and backgrounds in the analysis of $h \to \gamma\gamma$ are the same as in the Standard Model. As in the Standard Model case, this channels is not enough, by itself, to discover Higgs in the first years of LHC operation. However, the combination of inclusive $h \to \gamma\gamma$, with Wh and $ht\bar{t}$ associated production with a high p_T lepton, yields a discovery potential for $m_A > 180$ GeV/c^2 and $\tan\beta > 3$ at an integrated luminosity of 3×10^5pb^{-1} . The sensitivity is enhanced at lower $\tan\beta$ (see Figure 5).

The analysis for $h \to b\bar{b}$ is again identical as in the Standard Model case, where Wh events are tagged by a high-p_T lepton and the b-tag. The sensitivity for this particular mode is enhanced at low $\tan\beta$ ($\tan\beta$ <3

MSSM Particle	Main production modes	Decay modes	Experimental tag
h	h, Wh, tth	$h\to\gamma\gamma$ (SM)	Hi-p_T photons, btag
	Wh	$h\to b\bar{b}$ (SM)	Hi-p_T ℓ, btag
H	H	$H\to\gamma\gamma$ (SM)	Hi-p_T photons
	H	$H\to 4\ell$ (SM)	Hi-p_T isolated ℓ and btag veto
	WH	$H\to b\bar{b}$ (SM)	Hi-p_T ℓ, btag
	H	$H\to b\bar{b}\gamma\gamma$	Hi-p_T isolated ℓ's, btag
	H	$H\to\tau\tau$	Hi-p_T ℓ and hadron, $\not{E}_T$
A	A, $Ab\bar{b}$	$A\to\tau\tau$	Hi-p_T ℓ and hadron, $\not{E}_T$
	A	$A\to hZ\to\tau\tau$	Hi-p_T ℓ's, btag
$H^{\pm}$	$t\to Hb$	$H^{\pm}\to\tau^{\pm}\nu$	Hi-p_T ℓ, hi-p_T btag jets $\not{E}_T$

Table 1: Summary of main MSSM channels considered here. The modes labelled "SM" have identical topologies to the Standard Model Higgs.

and m_A >130 GeV/c^2) due to the higher hWW coupling at low $\tan\beta$. This is thus a good channel for low luminosity, as can be seen from Figure 4.

In the MSSM, only the heavy neutral Higgs H has a significant branching ratio to ZZ* and WW since m_H is too small and the pseudoscalar Higgs A does not couple at tree level. Thus, in the MSSM, the four-lepton channel is produced mainly via $H\to ZZ\to 4\ell$. In this case, the analysis is identical to the Standard Model analysis. This is an analysis best suited for high luminosity; significant portions of the parameter space start to be covered after three years of running. This channel also has good sensitivity at low $\tan\beta$ for $m_H < 2m_{top}$. For $m_H > 2m_{top}$, $H\to t\bar{t}$ dominates for low $\tan\beta$, as can be seen by the sudden drop in reach at $m_A \approx 2m_{top}$ in Figure 5 (here A and H are almost mass-degenerate).

5.3 SUSY-like channels

The $A/H\to\tau\tau$ channel is very important as it has good sensitivity to a large fraction of parameter space, even at low integrated luminosity. It is a challenging channel which requires very good detector resolution in $\not{E}_T$ in order to reconstruct $m_{\tau\tau}$. Di-tau events are selected by requiring two one-prong taus in an event. At least one of the taus must decay into a lepton; the other tau can decay leptonically or into a charged hadron. These requirements retain about 45% of di-tau events. The taus are identified as such by forming narrow high-p_T jets with one charged track only. This gives a tau identification efficiency of 26% and a jet rejection factor of 100. After using kinematic constraints to estimate the neutrino energies in the event, $m_{\tau\tau}$ is reconstructed with a resolution of $\sigma_m \approx 10\%$. This is a relatively "clean" channel: for $m_{A/H} \approx 200$ GeV/c^2 and $\tan\beta \approx 10$, the reach is $S/\sqrt{B} \approx 13$ for 3×10^4pb^{-1} . As can be seen for Figures 4 and 5, this Higgs mode covers a large fraction of the $\tan\beta - m_A$ plane. It is also evident from the figures the effect from the $Z\to\tau\tau$ background, which rises rapidly for low m_A .

When $m_{H^\pm} < m_{top}$, $H^\pm$ production proceeds through $t\to Hb$. The couplings are such that the branching ratio of $H^\pm\to\tau^\pm\nu$ is virtually 100%. The way to detect a $H^\pm$ signal is then to observe an excess of taus with respect to electrons and muons. Since a neutrino accompanies the tau, in this case it is not possible to reconstruct a $H^\pm$ mass peak. In this analysis, tau leptons are identified in the same way as in the $A/H\to\tau\tau$ channel. Events with an identified tau and a high-p_T isolated lepton with $|\eta| < 2.5$ are selected. In order to tag the initial $t\bar{t}$, events are also required to have three high-p_T jets, two of which must be b-tagged. The significance in this channel is dominated by a $\approx 3\%$ background uncertainty. For example, for $m_{H^\pm} = 130$ GeV/c^2 , $\tan\beta = 5$, $m_{top} = 175$ GeV/c^2 , and at 3×10^4pb^{-1} , 1550 signal events are expected with a total background of 7170 (W decays and fake taus). This gives, including the 3% systematic uncertainty, a reach of $S/\sqrt{B} \approx 6.6$

One of the most interesting MSSM Higgs decay modes is the $H\to hh$ channel, since it would imply the simultaneous observation of two Higgs bosons. In this case, $hh\to b\bar{b}b\bar{b}$ has the largest signal rates but also has very large reducible and irreducible QCD backgrounds [16]; this channel is under study. More promising is the $hh\to\gamma\gamma b\bar{b}$ channel. In this case, two isolated high-p_T photons are required in addition

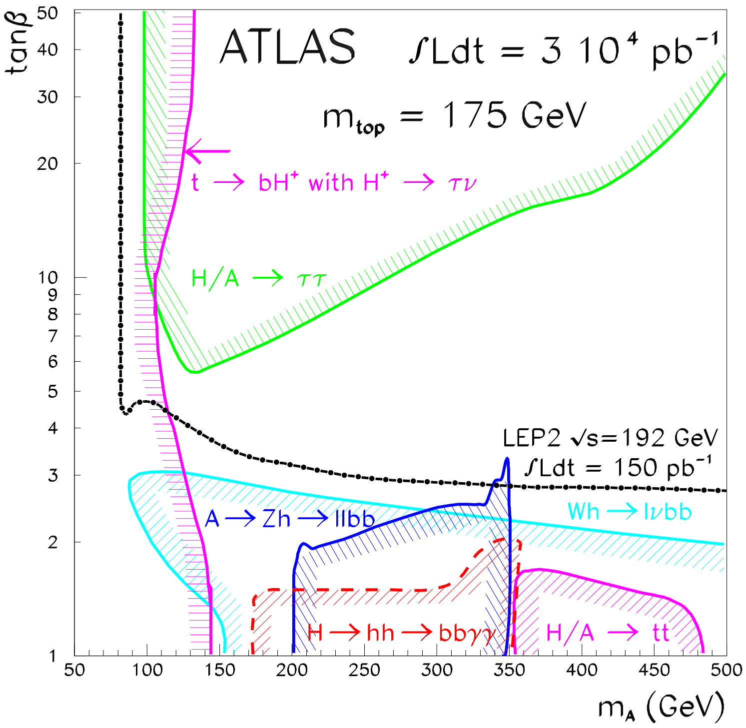

Figure 4: The 5σ ($S/\sqrt{B} \geq 5$) discovery $m_{\rm A}$-$\tan\beta$ contour for MSSM Higgs at 14 TeV for $m_{\rm top} = 175$ GeV/c^2 and 3×10^4pb^{-1}.

to two b-tagged jets. The good di-photon mass resolution gives very low backgrounds. However, this is a channel for high luminosity: for 3×10^5pb^{-1}, the expectations are 40 signal events and 2 background events. The resultant discovery contour is included in Figures 4 and 5. A similar channel is $\rm A\to Zh$. In this case the final state $\rm A\to Zh\to \ell\ell b\bar{b}$ is tagged by requiring two high-$p_{\rm T}$ leptons and two high-$p_{\rm T}$ b-tagged jets. After requiring the di-lepton pair mass to be consistent with $m_{\rm Z}$ and further constraining the events kinematically, the final sample contributes mostly to the low $\tan\beta$ region.

5.4 Conclusion on MSSM Higgs

If the MSSM is a valid description of nature, then for an integrated luminosity of 3×10^4pb^{-1}, ATLAS will probably discover at least one MSSM Higgs boson (Figure 4). For an integrated luminosity of 3×10^5pb^{-1}, ATLAS will probably discover several MSSM Higgs bosons. In these results, there are many systematic uncertainties which have not been addressed here. As already mentioned, K-factors are missing from both signal and background estimates. In addition there is a dependence on SUSY parameters and $m_{\rm top}$. On the experimental side, there are uncertainties on how the functionality of the detector elements is degraded with higher luminosity. This degradation directly affects quantities like isolation, $\not\!\!E_{\rm T}$, jet vetoes, and b-tagging capability. However, these discovery projections will improve with time as new, more accurate calculations become available and as the detector simulation and reconstruction algorithms are improved.

6 Supersymmetry

6.1 Introduction

Among other things, Supersymmetry addresses the hierarchy problem in the Standard Model. In SUSY, ordinary particles appear with their "spartners" in such a way that the number of fermionic and bosonic

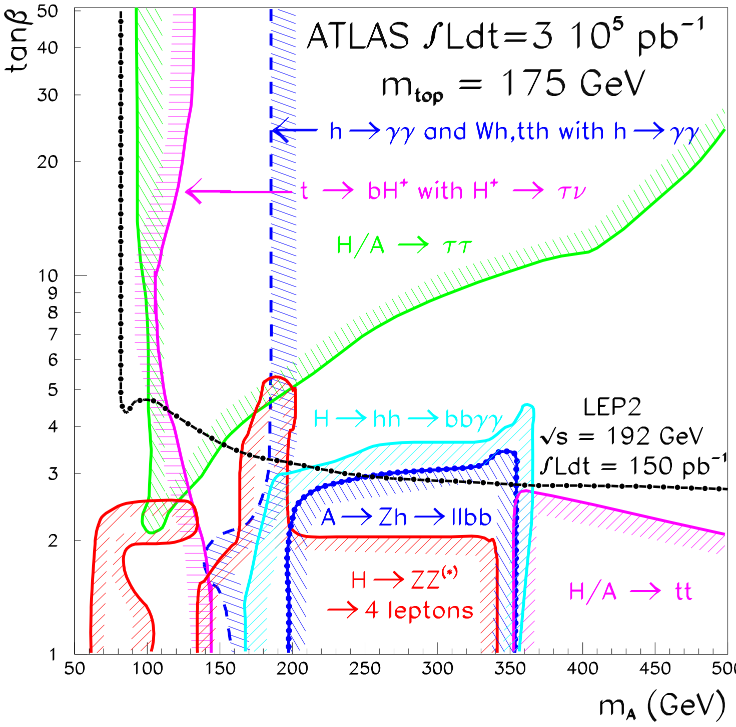

Figure 5: The 5σ $(S/\sqrt{B} \geq 5)$ discovery m_{A}-$\tan\beta$ contour for MSSM Higgs at 14 TeV for $m_{\mathrm{top}} = 175$ GeV/c^2 and 3×10^5pb^{-1}.

degrees of freedom is the same. The MSSM, discussed above in the context of the Higgs sector, is the minimal manifestation of SUSY consistent with the Standard Model.

The symmetrization of the degrees of freedom leads to a rich spectrum of new spin-0 (squarks and sleptons) and spin-$\frac{1}{2}$ particles. Many different implementations of SUSY exist. Among them, one that has been studied in some detail for the LHC [17], is the minimal supergravity model (mSUGRA). In this model, electrowek symmetry is radiatively broken and the weak, electromagnetic, and strong scales unify at the scale $M_{\mathrm{GUT}} \approx 10^{16}$ GeV/c^2. R-parity, the "SUSY-ness" quantum number, is conserved, implying that the lightest supersymmetric particle (LSP) is stable and weakly-interacting. This particle is usually taken to be the lightest neutralino, denoted by $\tilde{\chi}_1^0$.

Even in this relatively restricted model, there are four continuous and one discrete parameters: the universal scalar mass m_0, the universal gaugino mass $m_{\frac{1}{2}}$, the universal trilinear scalar coupling A_0, $\tan\beta$, and the sign of the Higgs-higgsino mass parameter $\mathrm{sign}(\mu)$. Since each point in the mSUGRA parameter space represents a phenomenologically different model, it is very difficult to build an analysis which efficiently covers all of the parameter space (*i.e.*, decay modes). However, SUSY particle masses, in the framework of mSUGRA, depend mostly on m_0 and $m_{\frac{1}{2}}$; thus m_0 and $m_{\frac{1}{2}}$ define the scalar and fermion particle mass scales.

At the turn-on of LHC, assuming no discovery, the TeVatron program [18] will will have set the lower limits for the SUSY scale at $\mathrm{M}_{\tilde{\mathrm{q}},\tilde{\mathrm{g}}} > 400$ GeV/c^2. If the h-Higgs is not found at LEP2, then low energy mSUGRA will be excluded [19] (low $m_{\frac{1}{2}}$). These constraints help in focusing the evaluation of SUSY prospects with ATLAS.

6.2 Discovering SUSY

SUSY events at the LHC will be copiously produced through strong processes, $\mathrm{pp}\to\tilde{\mathrm{g}}\tilde{\mathrm{g}}\mathrm{X}, \tilde{\mathrm{g}}\tilde{\mathrm{q}}\mathrm{X}, \tilde{\mathrm{q}}\tilde{\mathrm{q}}\mathrm{X}$ with typical cross sections that can range from 1 to 1000 pb. A clear excess in the total cross section could then be an indication for SUSY. In addition, since there are two $\tilde{\chi}_1^0$ in each mSUGRA final state, a clear experimental signature for SUSY is missing transverse energy $\not{E}_{\rm T}$. SUSY events also have many high-$p_{\rm T}$ jets, b-jets, and isolated leptons from the cascade decays of the high mass SUSY particles.

Since there is such a large dependence of the mSUGRA particle spectrum on the model parameters, studies at the LHC have concentrated on five SUGRA points selected for detailed study [17]. Here, as an illustration, we concentrate on Point 4, which corresponds to $m_0 = 800$ GeV/c^2 , $m_{\frac{1}{2}} = 200$ GeV/c^2 , $A_0 = 0$ GeV/c^2 , $\tan\beta = 10$, and sign$(\mu)=+$. The total cross section for SUSY production at this point is 30 pb.

Due to the generally large cross sections for SUSY processes at the LHC, any discovery of SUSY will probably be via inclusive distributions. Many experimental signatures of inclusive modes have been studied for discovery at the LHC [20]. These studies have been performed on fast detector simulations with a SUSY physics generator (ISAJET [21]). The experimental signatures investigated were the various combinations of multi-jets, multi-leptons (same, opposite charge), $\not{E}_{\rm T}$, jet vetoes, and lepton vetoes. These studies have shown that with an integrated luminosity of 10^4 pb^{-1} (first year of running), the multi-jets and $\not{E}_{\rm T}$ channels have the best reach. Thus, these modes will be emphasised during the first year of running.

In order to first establish SUSY and to identify its mass scale $\rm M_{SUSY}$ ($\rm M_{SUSY} \equiv \min(m_{\tilde{g}}, m_{\tilde{q}})$), it is convenient to simply analyze the event effective mass [22], defined as:

$$M_{\rm eff} = \not{E}_{\rm T} + p_{\rm T,1} + p_{\rm T,2} + p_{\rm T,3} + p_{\rm T,4}. \quad (1)$$

In the above, the $p_{\rm T,i}$ refer to the $p_{\rm T}$ of the four most energetic jets in the event. Standard Model background is reduced by requiring large $\not{E}_{\rm T}$, at least four high-$p_{\rm T}$ jets, no isolated high-$p_{\rm T}$ leptons, and a transverse sphericity of $S_{\rm T} > 0.2$. Figure 6 shows the effective mass distribution for mSUGRA Point 4 after the above requirements for one year of running at low luminosity. This figure would be a clear indication for SUSY. In addition, by generating “random SUGRA models”, studies have shown that the peak of the $M_{\rm eff}$ distribution is highly correlated with $\rm M_{SUSY}$.

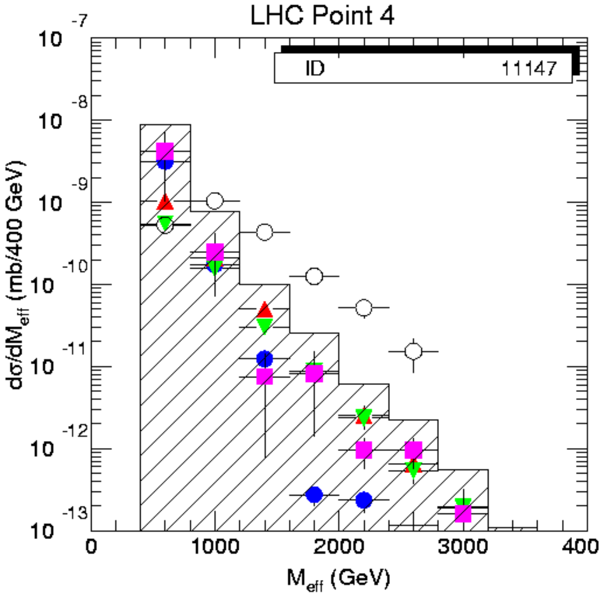

Figure 6: The effective mass distribution at LHC Point 4 [22]. The solid histogram is the sum of all Standard Model background contributions. The open circles are the SUSY signal contributions.

6.3 Extracting SUSY parameters

Once SUSY signatures are found and M_{SUSY} established, the next step is to try to differentiate between the different models. SUGRA-predicted masses, branching ratios, and cross sections are very model dependent. Exclusive measurements of SUSY signals can therefore be used to measure and constrain the model parameters.

Taking again as an example the SUGRA Point 4, the gluino mass is 582 GeV/c^2, the squark mass is 915 GeV/c^2, and the light Higgs mass is 111 GeV/c^2; since $m_{\tilde{q}} > m_{\tilde{g}}$, gluino production dominates. For $\tilde{g} \to q\bar{q}\tilde{\chi}_2^0$ (with a branching ratio of 27%), the next-to-lightest neutralino $\tilde{\chi}_2^0$ can decay to the LSP by $\tilde{\chi}_2^0 \to \ell^+\ell^-\tilde{\chi}_1^0$. By selecting events with two opposite-sign, same-flavor leptons and with additional SUSY-like requirements, the mass difference between the two lightest neutralinos can be extracted from the endpoint of the di-lepton mass distribution [23]. For an integrated luminosity of 3×10^4pb^{-1}, the mass difference can be measured to 1% while for 3×10^5pb^{-1} it can be measured to 0.2%.

Many other parameters can be extracted in a similar fashion. In a realistic scenario, these measurements would be used in turn to recursively predict other SUSY particle masses in order to further discriminate between the different models.

Experimental constraints like the ones described above from both inclusive and exclusive measurements can be used to "fit" mSUGRA model parameters [23]. This has been demonstrated by generating a very large number of models while varying the SUGRA parameters. A χ^2 is formed between each hypothetical model and an "experiment" (a fixed point in SUGRA parameter space) by comparing the "distance" between each model and experiment for all measurements. This χ^2 is then used to determine the allowed values of the model parameters as a function of integrated luminosity. For instance, at Point 4, m_0 can be determined to 6% and $m_{\frac{1}{2}}$ can be determined to 1%. After determining $\tan\beta$ and sign(μ) to similar precision, all particle masses can be predicted to an accuracy of 2–5%.

6.4 ATLAS Detector Issues

Since successful tagging of SUSY final states requires good $\not\!\!E_T$ resolution, it is important to understand any tails in the $\not\!\!E_T$ distribution due to detector effects. This tails ("instrumental background") arise mainly due to gaps in the detector coverage or due to detector regions with very poor resolution. Figure 7 shows the $\not\!\!E_T$ distribution for two M_{SUSY} scenarios [5]. It is clear that instrumental background can be safely ignored if a cut of $\not\!\!E_T > 100$ GeV is imposed in any SUSY analysis.

Energy scale uncertainties could also degrade the event reconstruction. However, in ATLAS, the various energy scales can be monitored and calibrated by using well-known physics processes. The muon energy scale can be established to 0.1% with Z and J/Ψ decays by using the Inner Detector and the muon system. The electron-photon energy scale can also be determined to 0.1% with Z and J/Ψ decays by using the electromagnetic calorimeter and the Inner Detector. The hadronic energy scale can be calibrated to 1% by using top decays and W$\to$jet-jet decays.

The ATLAS detector is thus capable of performing precision measurements in the LHC environment.

7 B Physics at ATLAS

The large cross section for $b\bar{b}$ production at $\sqrt{s} = 14$ TeV ($\sigma(pp \to b\bar{b}X) \approx 0.5$mb) makes the LHC a B factory. With the startup luminosity of 10^{33}cm^{-2}s^{-1}, this cross section translates into roughly 5×10^{12} $b\bar{b}$ expected events per year. Since B event reconstruction is very susceptible to pileup effects, the B physics program in ATLAS is only feasible during the low luminosity period. In addition, in order to unambiguously identify B final states, only fully reconstructible events will be accepted. The key to B physics at the LHC will thus be high selectivity.

A critical issue for B physics is triggering. The aim of the B trigger in ATLAS, part of the general three level trigger system, is to isolate final states which can be fully tagged. The level-1 trigger is simply the requirement of a muon with $p_T > 6$ GeV/c and $|\eta| < 2.2$ in the muon spectrometer. At this level, the trigger rate is already about 8 kHz at 60% purity. The level-2 trigger will reduce these rates even further by triggering on specific channels. For example, the decays $J/\Psi \to e^+e^-$, $B_d \to \pi^+\pi^-$, and $D_s \to \phi\pi$ will tag events as interesting B events. At this level many detector elements will be used (precision layers,

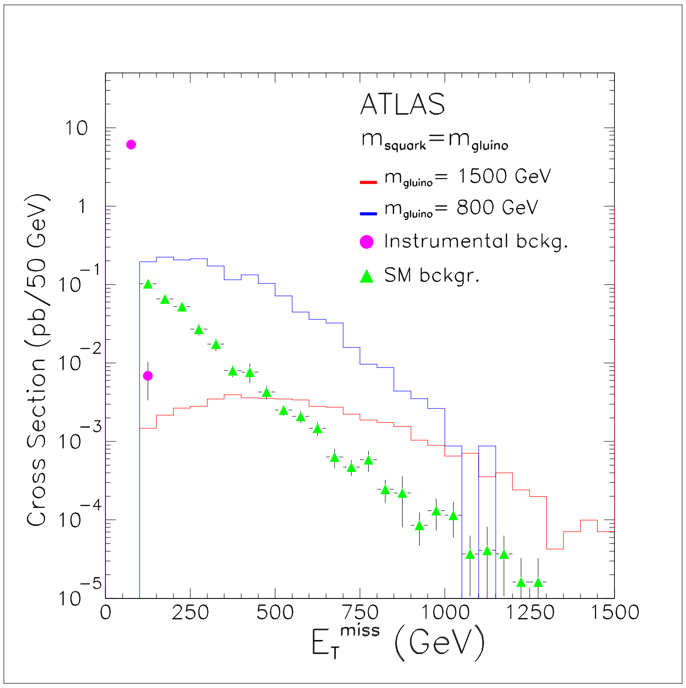

Figure 7: Contributions to $\not{E}_T$ from physics processes and detector effects. Instrumental effects are well below the Standard Model background for $\not{E}_T > 100$ GeV.

tracking, calorimeter) to reduce the trigger rate to about 500–600 Hz. A level-3 trigger will further refine the selection down to about 100 Hz.

One of the most important aims of B physics at the LHC is the study of CP violation in the context of the Standard Model. The measurement of the unitarity triangle parameters will help in the understanding of the origin of CP violation.

The CP eigenstate decay $B_d \to J/\Psi K_s$ will be used to measure the CP violating parameter $\sin 2\beta$ via the decay asymmetry,

$$A(t) = \frac{N_B(t) - N_{\bar{B}}(t)}{N_B(t) + N_{\bar{B}}(t)} = \sin 2\beta \sin(x_d \Gamma t). \tag{2}$$

After tagging the flavor (B or $\bar{B}$) by using the charge of the lepton on the "other side", the $B_d \to J/\Psi K_s$ side is fully reconstructed and mass cuts are applied. The prospects for $10^4 pb^{-1}$ (first year of operation) are approximately 21,000 $B_d \to J/\Psi K_s$ events with 4,200 background events [24]. This translates into a reach of $\delta(\sin 2\beta) \approx 0.021$ (statistical only) for a time-integrated asymmetry measurement. A time-dependent measurement can improve this reach by roughly 15%. In addition, other tagging methods under study will improve the reach, namely, B^{**} tagging and jet-charge tagging. Systematic uncertainties can be studied with the analogous decays $B^+ \to J/\Psi K^+$ and $B_d \to J/\Psi K^{0*}$.

The parameter $\sin 2\alpha$ can similarly be measured with the decay asymmetry of $B_d \to \pi^+\pi^-$. The statistical reach for this channel is $\delta(\sin 2\alpha) \approx 0.043$; however, there are theoretical ambiguities which make the evaluation of systematic uncertainties very difficult.

The measurement of the B_s mixing parameter x_s in ATLAS [25] can be used to infer the value of the ratio of CKM matrix elements $|V_{ts}/V_{td}|^2$. The excellent proper time resolution of the ATLAS tracker ($\delta\tau \approx 0.07$ ps) is essential in the measurement of x_s. In this case, the fully reconstructed final states $D_s\pi$, $D_s a_1$ are used to tag the B_s initial state. Figure 8 shows the result of a $x_s = 37$ measurement after one year of running at low luminosity. The ATLAS reach is $x_s < 40$

In addition to the above measurements, ATLAS will also pursue the search and measurement of rare B decays, which provide an independent test of the Standard Model.

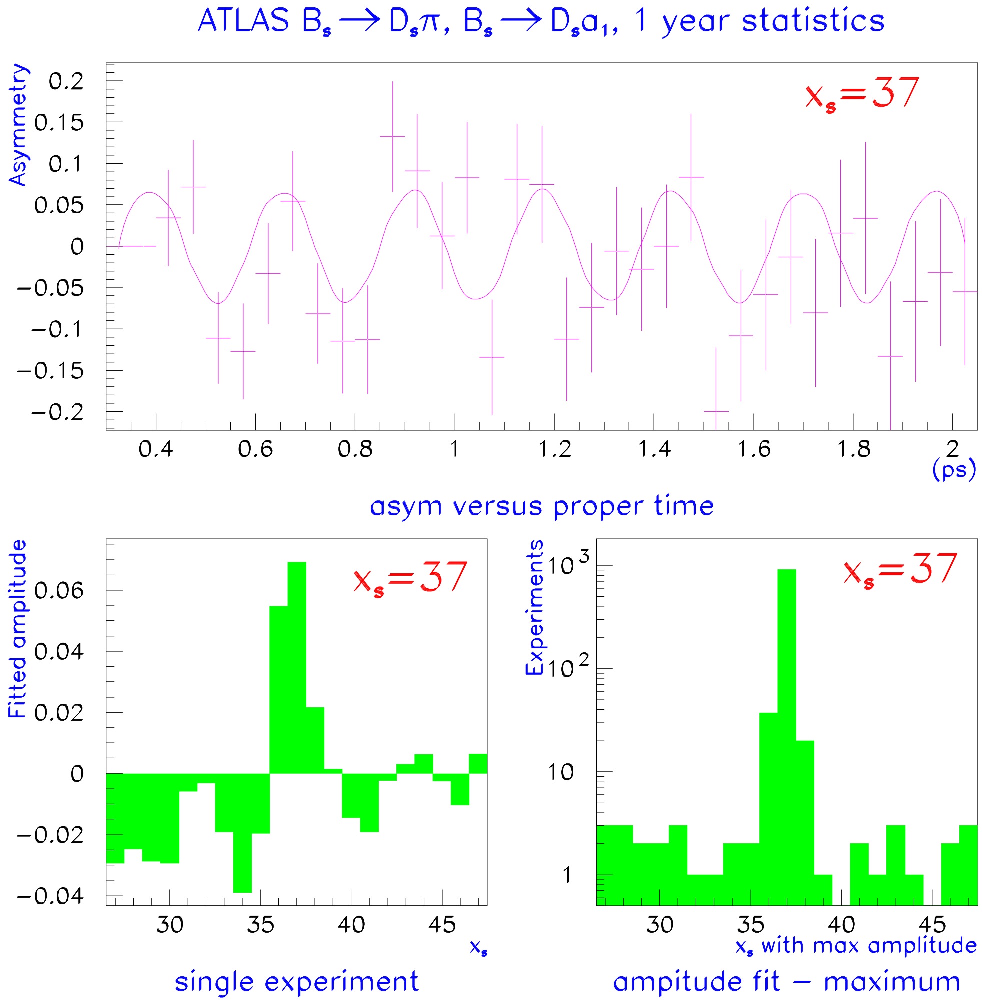

Figure 8: Measurement of the B_s mixing mixing parameter x_s at ATLAS.

8 Conclusion

ATLAS will discover the Standard Model Higgs Boson if it exists in the mass range $m_H < 1$ TeV/c^2. ATLAS also has a good chance of discovering at least on MSSM Higgs boson during the first years of operation. Essentially all of the allowed MSSM parameter space will be covered after years of high luminosity running.

If supersymmetry exists at the electroweak scale, it will then be found at the LHC. The SUSY scale will be determined up to 2 TeV/c^2 and precision measurements will allow distinguishing between different SUSY models.

ATLAS will also pursue a vigorous B physics effort at the beginning of LHC operation, in particular in probing the origins of CP violation.

These topics, and many others not covered in this talk, will ensure that ATLAS will have a vigorous physics life at the LHC.

9 Acknowledgements

I wish to thank the organizers for providing a stimulating atmosphere and a very interesting Workshop. I also wish to thank Daniel Froidevaux and Paula Eerola for their help in collecting some of the ATLAS

physics performance results. I also wish to thank all of my ATLAS collaborators whose hard work is presented here.

References

[1] T. Sjöstrand, Comput. Phys. Commun. 82 (1994) 74.

[2] M. Spira, Preprint CERN-TH-97-0335, March 1997.

[3] *The LHC Conceptual Design Report*, CERN/AC/95-05 (LHC), October 1995.

[4] ATLAS Collaboration, *ATLAS Technical Design Report* CERN/LHCC 96-40 to CERN/LHCC 96-43 and CERN/LHCC 97-16 to CERN/LHCC 97-22.

[5] ATLAS Technical Proposal, CERN/LHCC/94-43, LHCC/P2 (15 December 1994)

[6] A. Henriques, *Status of the ATLAS detector*, talk given at this Workshop, September 1997.

[7] LEP working group for Higgs boson searches, *Lower bound for the SM Higgs boson mass: combined results from the four LEP experiments,* CERN-LEPC/97-11 (November 1997).

[8] G. Altarelli, Preprint CERN-TH-97-278, October. 1997.

[9] S. Kim *et al.*, Preprint CDF/ANAL/EXOTIC/PUBLIC/3904, October 1996.

[10] Z. Kunszt, S. Moretti, W.J. Stirling, Preprint ETH-TH/96-48, September 1996.

[11] V. Tisserand, ATLAS Internal Note PHYS-No-90, July 1996.

[12] O. Linossier, L. Poggioli, ATLAS Internal Note PHYS-No-101, April 1997.

[13] E. Richter-Wąs *et al*, ATLAS Internal Note, PHYS-No-074, April 22, 1996

[14] M. Carena *et al.*, Phys. Lett. B355 (1995) 209.

[15] T. Greening, *Searches for the MSSM Higgs Boson al LEP*, talk given at *Physics at the First Muon Collider* Workshop, Betavia, Nov 6–9, 1997.

[16] E. Richter-Wąs, D. Froidevaux, Z. Phys. C76 (1997) 665.

[17] A. Bartl *at al.*, Preprint LBNL-39413, November 1996.

[18] H. Baer *at al.*, Preprint FSU-HEP-960415 (hep-ph/9604406) (April 1996)

[19] D. Froidveaux, *SUSY at the LHC*, talk given at *International Workshop on New Physics in Non-Accelerator Experiments*, Dubna (July 7–11, 1997).

[20] H. Baer *at al.*, Preprint FSU-HEP-950204 (hep-ph/9503271) (March 1995).
H. Baer *at al.*, Preprint FSU-HEP-951215 (hep-ph/9503383) (December 1995).

[21] H. Baer *at al.*, in *Proceedings of the Workshop on Physics at Current Accelerators and Supercolliders* ed. J. Hewitt, A. White, and D. Zeppenfeld (ANL 1993).

[22] I. Hinchliffe *at al.*, Phys. Rev. D55 (1997) 5520.

[23] D. Froidevaux, F. Gianotti, G. Polesello, Talks at *LHCC Workshop on Supersymmetry* CERN (October 30, 1996)

[24] P. Eerola, Preprint ETH-TH/96-48, September 1996.

[25] S. Gadomski *et al.*, Preprint HU-SEFT R 1996-21, October 1996.